

REDUCING INSTRUMENTATION ERRORS CAUSED BY CIRCUMFERENTIAL FLOW FIELD VARIATIONS IN MULTI-STAGE AXIAL COMPRESSORS

M. Chilla, G. Pullan

Whittle Laboratory, University of Cambridge
Cambridge, United Kingdom

S. Gallimore

Rolls-Royce plc.
Derby, United Kingdom

ABSTRACT

The effects of blade row interactions on stator-mounted instrumentation in axial compressors are investigated using unsteady numerical calculations. The test compressor is an 8-stage machine representative of an aero-engine core compressor. For the unsteady calculations, a 180deg sector (half-annulus) model of the compressor is used.

It is shown that the time-mean flow field in the stator leading edge planes is circumferentially non-uniform. The circumferential variations in stagnation pressure and stagnation temperature respectively reach 4.2% and 1.1% of the local mean. Using spatial wave number analysis, the incoming wakes from the upstream stator rows are identified as the dominant source of the circumferential variations in the front and middle of the compressor, while towards the rear of the compressor, the upstream influence of the eight struts in the exit duct becomes dominant. Based on three circumferential probes, the sampling errors for stagnation pressure and stagnation temperature are calculated as a function of the probe locations. Optimization of the probe locations shows that the sampling error can be reduced by up to 77% by circumferentially redistributing the individual probes. The reductions in the sampling errors translate to reductions in the uncertainties of the overall compressor efficiency and inlet flow capacity by up to 50%.

Recognizing that data from large-scale unsteady calculations is rarely available in the instrumentation phase for a new test rig or engine, a method for approximating the circumferential variations with single harmonics is presented. The construction of the harmonics is based solely on the knowledge of the number of stators in each row and a small number of equi-spaced probes. It is shown how excursions in the sampling error are reduced by increasing the number of circumferential probes.

INTRODUCTION

In multi-stage axial compressor rig or engine tests, probes are typically mounted on a few selected stators of each stage to acquire time-mean stagnation pressure (P_0) and stagnation temperature (T_0) data throughout the machine. These instrumented stators are distributed around the annulus. Their circumferential location is typically chosen to avoid the wake paths of the upstream instrumented stators. Each instrumented stator typically includes probes at several radial heights. A probe configuration with five radial probes (P_0) on three instrumented stators around the annulus is schematically shown in Figure 1.

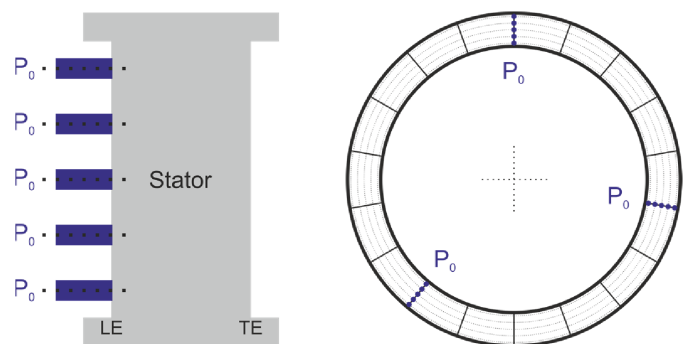


Figure 1: Schematic illustration of radial and circumferential positions of stator leading edge probes (P_0) during a rig or engine test

The time-mean flow field in a multi-stage axial compressor at design operating conditions is circumferentially non-uniform [4], [7], [12]. The flow field is affected by the wakes from the upstream stator rows and the potential fields of the adjacent

stationary components. Consequently, the local reading of stagnation pressure or stagnation temperature depends on the position of the instrumented stator relative to the surrounding vanes. The circumferential average of the discrete probe readings generally differs from the true circumferential average taking the complete flow field into account. The consequence is a systematic probe sampling error. There are other errors associated with a probe's evaluation of the local values of stagnation pressure and stagnation temperature, e.g. due to the probe's response to incidence. However, in this paper the effect of circumferential flow non-uniformities as measured by an ideal probe is assessed. To this end, CFD calculations are used as numerical experiments in support of a physical multi-stage compressor rig test. In contrast to the physical test, in the CFD the complete set of flow field data is available. The objectives of this paper are to:

- Define the sampling error as a metric for the difference between the mean of a set of circumferential samples and the true circumferential mean;
- Identify the causes of the circumferential non-uniformities in the time-averaged stagnation pressure and stagnation temperature;
- Quantify the magnitudes of the circumferential variations in the time-averaged stagnation pressure and stagnation temperature;
- Quantify the sampling error for the probe arrangement that was used during a representative physical compressor rig test;
- Identify the probe arrangement which results in the smallest possible sampling error, and to quantify the associated reduction in sampling error relative to the datum probe arrangement;
- Quantify the effect of the sampling errors in stagnation pressure and stagnation temperature on compressor performance assessment;
- Develop a generally applicable method for the circumferential positioning of stator-mounted probes, which is based only on the knowledge of the number of stators in each row and can therefore be used during the early stages of a compressor test program.

To achieve these objectives, the paper is organized in the following way. At first, the numerical model of the multi-stage compressor is described. Following that, the approach of evaluating the sampling error for the datum probe arrangement is presented. Using a search algorithm on the CFD data, the probe positions which give the smallest possible sampling error are identified and the datum and minimum sampling errors are compared. The effect of the sampling error on compressor performance parameters is evaluated. In the final part of the paper, a method of using single harmonics to approximate the actual circumferential variations is presented. An assessment of

the effect of the number of circumferential probes on the resulting sampling error is given.

NOMENCLATURE

Symbols

C	Flow capacity [$s \cdot m \cdot \sqrt{K}$]
h	Non-dimensional radial height [%]
\dot{m}	Mass flow rate [kg/s]
p	Static pressure [Pa]
P_0	Stagnation pressure [Pa]
r	Radial coordinate [m]
T_0	Stagnation temperature [K]
x	Axial coordinate [m]
y^+	Non-dimensional wall distance [-]
α_m	Meridional flow angle [deg]
α_t	Tangential flow angle [deg]
γ	Ratio of specific heat capacities [-]
Δ	Change in quantity [-]
ε	Sampling error [%]
η	Efficiency [%]
θ	Circumferential coordinate [rad, deg]
ρ	Density [kg/m^3]

Indices

0	Stagnation quantity
avg	Average value
design	Design operating condition
ex	Exit station
in	Inlet station
mass	Mass-averaged value
max	Maximum value
min	Minimum value
samp	Probe sample
signal	Circumferential signal (CFD)

Abbreviations

CFD	Computational Fluid Dynamics
CPU	Central Processing Unit
ESS	Engine Section Stator
GPU	Graphics Processing Unit
IGV	Inlet Guide Vane
IPC	Intermediate Pressure Compressor
LE	Leading Edge
PR	Pressure Ratio
RANS	Reynolds-Averaged Navier-Stokes
S	Stator
SND	Swan-Necked Duct
TR	Temperature Ratio

NUMERICAL MODEL

The test compressor is an 8-stage high-speed machine, representative of modern aero-engine multi-stage core compressors. It is the same compressor as described by Dodds

and Vahdati in [2] and [3] and investigated by Wang et al. in [13]. Upstream of the eight stages of rotating and stationary blade rows an engine section stator (ESS) and an inlet guide vane (IGV) are located. At the exit of the compressor is a swan-necked duct (SND), which houses eight struts distributed uniformly around the annulus. The inlet guide vane, as well as the first three stator rows, are designed to be variable. The test compressor is shown schematically in the meridional (x - r) plane in Figure 2. The numerical model includes ducts at the inlet and exit of the domain in order to reduce unphysical coupling between the unsteady compressor flow and the domain boundaries. The length of the ducts is one quarter of the local annulus circumference. For clarity, the inlet and exit ducts are omitted in Figure 2. The numerical model also includes detailed geometry features, which are of engine-representative size. The rotor tip gaps as well as the penny gaps of the variable stator vanes are meshed and endwall fillets are included in all blade rows.

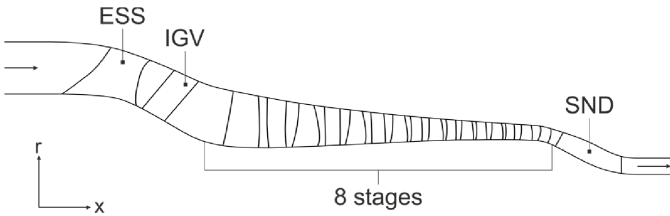


Figure 2: Schematic of the test compressor, including the engine section stator (ESS) and the inlet guide vane (IGV) at the front and the swan-necked duct (SND) strut at the rear

For the unsteady calculations, a 180deg circumferential sector of the compressor was modelled. The test compressor has an even number of rotor blades and stator vanes in each row, except for one blade row. For the row with the uneven number of blades, a single blade was added and the blade pitch reduced by 1.4% to match the circumferential sector size.

The numerical domain was discretized with a block-structured mesh, which was generated using the Rolls-Royce in-house code PADRAM [10]. For each blade passage, an O-4H mesh topology is used. Additional mesh blocks are used to resolve the gaps at the rotor tips and at the endwalls of the variable stator vanes. Between 0.5 and 1.3 million mesh points are used per blade passage, resulting in around 15 million mesh points for the single-passage model and around 450 million mesh points for the half-annulus (180-degree sector) model. The mesh is clustered towards the viscous surfaces to achieve values of the non-dimensional wall distance within the laminar sublayer of the boundary layer ($y^+ < 5$). As examples, the surface meshes of rotor-6 and stator-6 as well as the penny gap mesh at the tip of stator-1 and the tip gap mesh of rotor-8 are shown in Figure 3. The Spalart-Allmaras model [11] with helicity correction [9] is used to capture the effects of turbulence. The turbulence model is used in combination with adaptive wall functions, which operate in

the log-law region as well as in the sublayer region of the boundary layer.

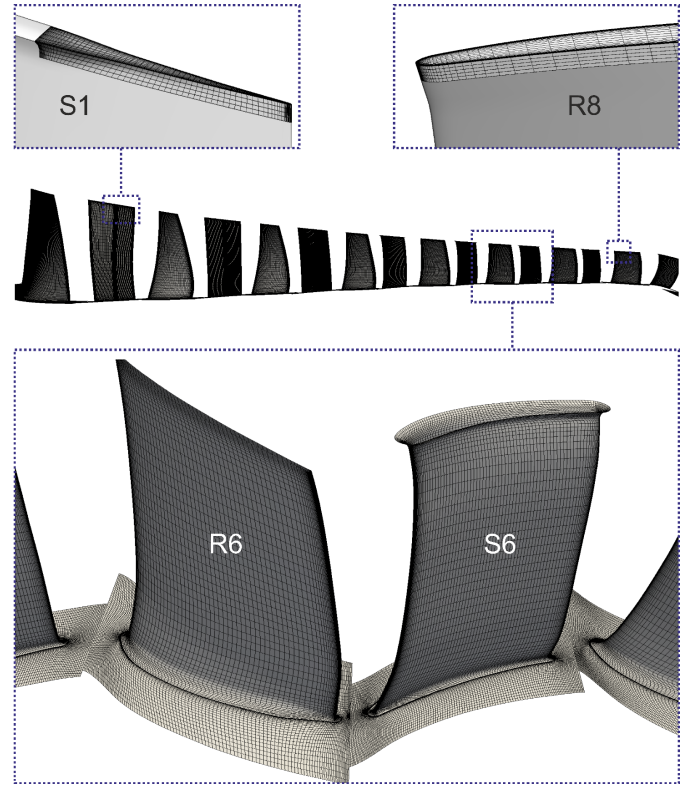


Figure 3: Details of the numerical mesh: surface and hub of rotor-6 and stator-6, tip penny gap of stator-1 and tip gap of rotor-8

As flow boundary conditions, radial profiles of stagnation pressure, stagnation temperature, meridional flow angle and tangential flow angle were specified at the inlet of the numerical domain. At the exit, a value for the static pressure at the casing together with the radial equilibrium condition was set. The operating point of the compressor was varied by changing the static pressure at the domain exit boundary. None of the operating points considered in this study was set at the stability boundary of the compressor, therefore permitting the assumption of the 180-degree flow periodicity. The stationary and rotating domains of the unsteady model were connected via sliding plane interfaces. At the interfaces, one-to-one point connections in the meridional (x - r) plane were ensured. The interface treatment is non-reflective.

The CFD calculations were conducted with the GPU flow solver Turbostream [1] version 3 on the Wilkes-2 cluster [14]. Turbostream version 3 is a structured multi-block RANS solver, which is second order accurate in space and time. The flow equations are solved using the finite-volume method with node-storage. For the time-wise integration, a dual time-stepping technique is used [6]. The code has been previously used for

steady and unsteady calculations of several gas turbine representative compressor rotors and fans [5], [8].

To initialize the flow field for the unsteady calculations, a converged solution of a steady single-passage calculation with mixing-plane blade row interfaces was used. During the unsteady calculations, the mass flow ratio (\dot{m}_2/\dot{m}_1) and the efficiency (η) of the compressor were monitored to evaluate convergence. The parameters were found to be settled after three shaft revolutions, which is equivalent to 1.5 domain throughflow times. At that stage, the peak-to-peak variation of the limit cycle was 0.2% for the mass flow ratio and 0.03% for the efficiency. Data was extracted only after the calculations had reached the converged state. Using 48 GPUs on the Wilkes-2 cluster, half a revolution could be calculated within one day, allowing the data extraction from the unsteady model to start after less than a week of running.

CIRCUMFERENTIAL VARIATIONS OF STAGNATION PRESSURE AND STAGNATION TEMPERATURE

The data of interest for this study is located at the stator leading edges of the multi-stage compressor. The focus is placed on the mid-span (50% height) probes. The location of the stator leading edge planes is indicated in Figure 4 on a mid-span contour of instantaneous entropy. From the unsteady calculation, the time-average flow field is calculated by averaging over half a shaft revolution. The circumferential data of interest at the stator leading edges is then extracted from the time-averaged solution. Examples of the extracted time-averaged data are shown in Figure 5 for the stagnation pressure and stagnation temperature at mid-span at the leading edge of stator-6. Since the data from the numerical model only covers a 180-degree sector, it is duplicated to cover the full circumference. The circumferential signals are shown as variations from the mean value, normalized by the mean value. The normalized variations in stagnation pressure are larger than those of the stagnation temperature. The circumferential signals are shown to contain low as well as high wave number content. The exact wave number composition of the circumferential signals at the stator leading edges will be discussed in more detail in the following sections.

For all eight stator rows of the compressor, the circumferential peak-to-peak variations in the non-dimensional stagnation pressure and stagnation temperature at mid-span are summarized in Table 1. The stagnation pressure varies between 2.7% and 4.2% of the local mean and the stagnation temperature between 0.6% and 1.1% of the local mean. The variations in the stagnation pressure are particularly high at the front of the compressor (S1), at the leading edge of stator-6 and at the rear of the compressor (S8). The variations in the stagnation temperature are relatively constant through the stator rows, increasing only at the rear of the compressor, just upstream of the large struts in the swan-necked exit duct.

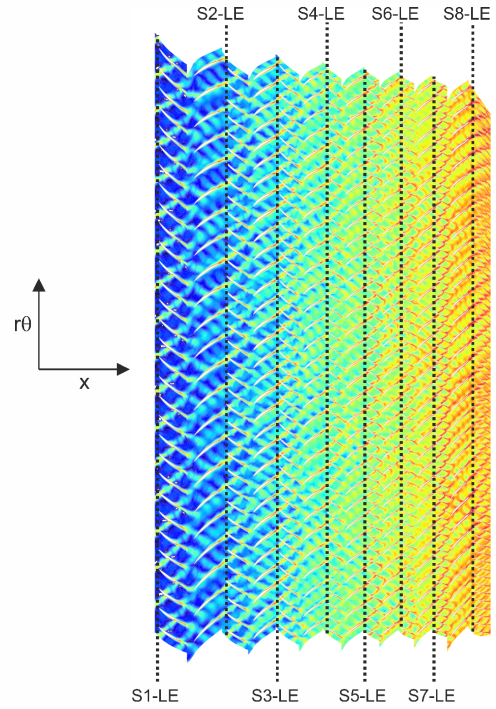


Figure 4: Stator leading edge positions indicated on instantaneous entropy contour at mid-span, unsteady 180deg sector calculation at design operating conditions

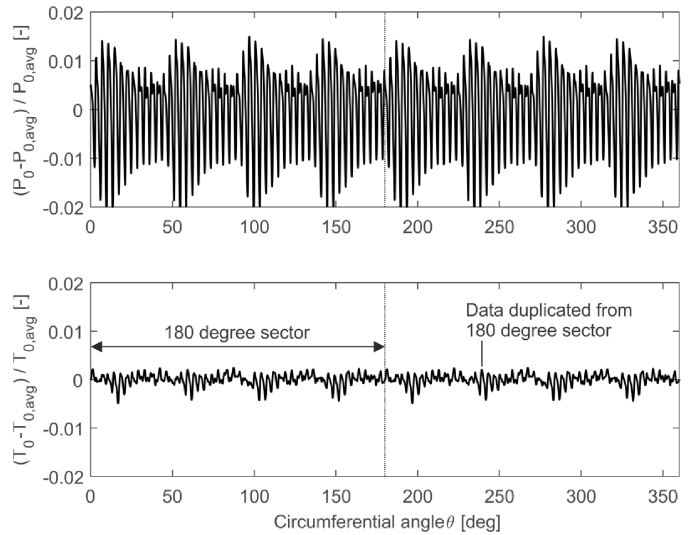


Figure 5: Circumferential signals of non-dimensional stagnation pressure and stagnation temperature at stator-6 leading edge (design operating condition, 50% height)

Table 1: Peak-to-peak variations of stagnation pressure (P_0) and stagnation temperature (T_0) at stator leading edges at 50% height

Stator row	$(P_{0,max}-P_{0,min})/P_{0,avg}$ [%]	$(T_{0,max}-T_{0,min})/T_{0,avg}$ [%]
S1	3.9	0.7
S2	2.7	0.7
S3	2.7	0.7
S4	2.8	0.6
S5	2.7	0.7
S6	3.7	0.7
S7	3.2	0.8
S8	4.2	1.1

From the extracted circumferential signals, wave number spectra were calculated using Fourier decomposition. The wave number spectra for the stagnation pressure and the stagnation temperature signals are shown in Figure 6 and Figure 7, respectively.

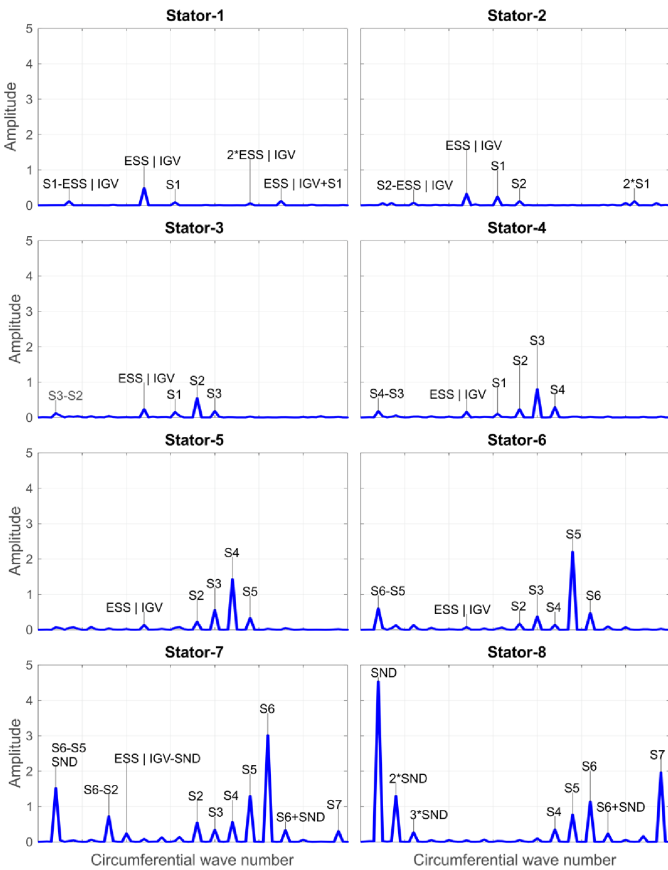


Figure 6: Circumferential wave number spectra of stagnation pressure at stator leading edges (design operating conditions, 50% height)

The spectra show clear peaks at the wave numbers associated with the stator wakes and the SND-strut pressure field. In addition to the fundamental harmonics, higher harmonics as well as combinations of two harmonics are shown. Considering the stagnation pressure spectra in Figure 6 first, the wave number associated with the ESS|IGV-wake pattern is dominant at the leading edges of stator-1 and stator-2. The ESS-wake pattern and the IGV-wake pattern are combined in this case, since the present compressor has the same number of engine section stators and inlet guide vanes. At the leading edge of stator-2, the stator-1 wake wave number is also prominent, but has a smaller wave number than the ESS|IGV-wake pattern. For the stator leading edges 3-7, the wave number with the largest amplitude is associated with the wake pattern from the stator row immediately upstream. In addition, the circumferential wave numbers of the local stator row and of stator rows further upstream are also present. At the rear of the compressor, the upstream influence of the large exit struts in the swan-necked duct becomes significant. The pressure field from the struts extends upstream and causes a locally higher static pressure at the exit of rotor-8. Due to this increased back-pressure rotor-8 locally operates higher on its characteristic. Consequently, the stagnation pressure at the leading edge of stator-8 is increased upstream of each of the SND-struts. At the leading edge of stator-8, the wave number associated with the SND-strut potential field is shown to have the largest local amplitude. This amplitude is more than twice as large as the one associated with the wake-pattern of stator-7.

For the stagnation temperature, the wave number associated with the upstream wake-pattern is dominant at the leading edges of stator-1 to stator-5. Towards the rear of the compressor, combinations of fundamental wave numbers become more prominent, e.g. the difference of the S5 and S4 harmonics at the leading edge of stator-5 or the difference of the S6 and S5 harmonics at the leading edge of stator-6. The signals at the leading edges of stator-7 and stator-8 are dominated by the upstream influence of the SND-struts. The effect of the locally back-pressured rotor-8 is detected in the circumferential variations of the stagnation temperature. Compared to the stagnation pressure spectra, the wave number content in the stagnation temperature spectra increases. At most of the stator leading edges several dominant wave numbers are present. This has implications for the approximation of the circumferential signals with individual harmonics, which is further discussed in the final part of this paper.

SAMPLING OF CIRCUMFERENTIAL VARIATIONS AT DISCRETE LOCATIONS

In the previous section, the circumferential flow variations at the stator leading edges have been characterized in terms of their magnitude and their wave number content. In this section, the error associated with the circumferential sampling of the flow field at discrete locations is discussed. The sampling of the circumferential variations at three discrete locations is illustrated in Figure 8. The circumferential stagnation pressure signal at

stagnation pressures are generally larger than those for the stagnation temperatures, which is driven by the larger circumferential variations present in the stagnation pressure signals. For the datum probe locations, the sampling error ranges between 0.18-0.42% for the stagnation pressure and between 0.03-0.06% for the stagnation temperature. Circumferentially redistributing the three probes from their datum to their optimum positions reduce the sampling error. For the optimum locations of three circumferential probes, the sampling error reduces to 0.07-0.36% for the stagnation pressure and to 0.02-0.05% for the stagnation temperature. By introducing more circumferential probes, the sampling error can be further reduced. With five circumferential probes, the minimum sampling error is predicted to reduce to between 0.02-0.30% for the stagnation pressure and to between 0.01-0.05% for the stagnation temperature.

EFFECT OF SAMPLING ERRORS ON PERFORMANCE

In the previous section, the sampling errors for the datum probe configuration with three circumferential probes and for the probe configurations with the smallest sampling error for three, four and five circumferential probes, have been calculated. In this section, the effect of the sampling error on the performance assessment of the compressor is presented. As performance parameters, the isentropic efficiency and the flow capacity are used. As previously described, the sampling error is related to the difference between the average of the individual samples and the average of the full circumferential signal via Equation (1). This relationship can be rewritten for the stagnation pressure and the stagnation temperature as follows:

$$\Delta P_0 = \varepsilon \cdot \overline{P_{0,\text{signal}}} \quad \Delta T_0 = \varepsilon \cdot \overline{T_{0,\text{signal}}}$$

These relations show that at a constant sampling error, the difference between the sample-average and the signal average scales with the mean pressure or temperature level. By adding or subtracting these differences to or from the mean values, the maximum and minimum pressure and temperature ratios can be calculated. The pressure and temperature ratios are defined between an inlet station ('in') and an exit station ('ex') and can be written as:

$$\begin{aligned} PR_{\max} &= \frac{\overline{P_{0,\text{ex}}} + \Delta P_{0,\text{ex}}}{\overline{P_{0,\text{in}}} - \Delta P_{0,\text{in}}} & TR_{\max} &= \frac{\overline{T_{0,\text{ex}}} + \Delta T_{0,\text{ex}}}{\overline{T_{0,\text{in}}} - \Delta T_{0,\text{in}}} \\ PR_{\min} &= \frac{\overline{P_{0,\text{ex}}} - \Delta P_{0,\text{ex}}}{\overline{P_{0,\text{in}}} + \Delta P_{0,\text{in}}} & TR_{\min} &= \frac{\overline{T_{0,\text{ex}}} - \Delta T_{0,\text{ex}}}{\overline{T_{0,\text{in}}} + \Delta T_{0,\text{in}}} \end{aligned}$$

The isentropic efficiency can be calculated as a function of the pressure and temperature ratios. From the maximum and minimum values of the pressure and temperature ratios, the maximum and minimum values of the isentropic efficiency are calculated as follows:

$$\eta_{\max} = \frac{\overline{PR}_{\max}^{\frac{\gamma-1}{\gamma}} - 1}{\overline{TR}_{\min} - 1} \quad \eta_{\min} = \frac{\overline{PR}_{\min}^{\frac{\gamma-1}{\gamma}} - 1}{\overline{TR}_{\max} - 1}$$

In the same way, the maximum and minimum values for the stagnation pressure and stagnation temperature are used to calculate the maximum and minimum values of the flow capacity (C). While the efficiency is calculated between two stations, the flow capacity is calculated at a single station. Therefore, the flow capacity is only affected by the P_0 and T_0 errors at one station, while for the calculation of the efficiency, the errors at two stations combine.

$$C_{\max} = \frac{\dot{m} \cdot \sqrt{T_{0,\max}}}{P_{0,\min}} \quad C_{\min} = \frac{\dot{m} \cdot \sqrt{T_{0,\min}}}{P_{0,\max}}$$

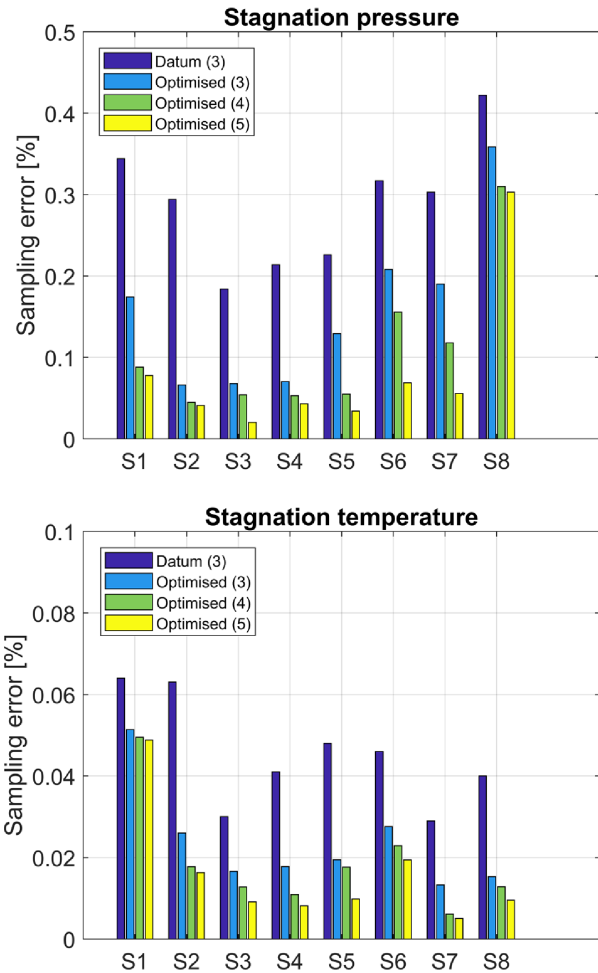


Figure 9: Comparison of sampling errors due to circumferential variations in stagnation pressure and stagnation temperature (design operating conditions, 50% height)

The calculated error ranges for the efficiency and the normalized inlet flow capacity are shown in Figure 10 for three operating points. In addition to the design operating point, data for a high flow capacity condition and a low flow capacity condition are shown. The error ranges are given for the datum probe arrangement with three circumferential probes as well as for the optimized probe arrangements using three, four and five circumferential probes. For each of the three operating conditions, the optimization of the probe positions was conducted individually. The identified optimum positions are therefore not the same for the three operating points. They are used solely to determine the theoretically possible error ranges.

Figure 10(a) shows the data calculated between the leading edge of stator-1 and the leading edge of stator-8, giving the overall performance of the compressor. At all three operating conditions, the error range for the inlet capacity is shown to be around 0.8% for the datum probe arrangement. When rearranging the three circumferential probes from their datum to their optimum positions, the error range reduces to 0.4%. With five circumferential probes at their optimum positions, the error range of the inlet capacity reduces to around 0.2%. The error ranges for the efficiency at the design and the low-flow operating condition are between 1.5% for the datum probe arrangement and 0.6% for the optimum probe arrangement of five circumferential probes. For the high-flow operating condition, the error ranges for the efficiency increase to between 2.8% for the datum probe arrangement and 1.4% for the optimum arrangement of five circumferential probes. The error ranges for the overall performance parameters, evaluated between the leading edges of S1 and S8, are summarized in Table 2.

Table 2: Error ranges for overall (S1-S8) isentropic efficiency and inlet flow capacity due to sampling errors in P_0 and T_0

a) Inlet flow capacity (normalized) [%]				
Condition	Datum (3)	Opt (3)	Opt (4)	Opt (5)
Low-flow	0.7	0.4	0.4	0.3
Design	0.8	0.4	0.2	0.2
High-flow	0.8	0.4	0.2	0.2

b) Isentropic efficiency [%]				
Condition	Datum (3)	Opt (3)	Opt (4)	Opt (5)
Low-flow	1.4	0.8	0.7	0.6
Design	1.5	1.0	0.8	0.8
High-flow	2.8	1.6	1.4	1.4

In addition to the overall performance, the block performance for the front (S1-S2), middle (S4-S5) and rear (S7-S8) blocks are shown in subplots (b)-(d) of Figure 10. As the local sampling errors are reduced by optimizing the probe

positions and by using more circumferential probes, the error ranges of the block performance parameters are progressively reduced. According to Equation (1), the sampling error changes proportionally to the difference of the sample mean from the true circumferential mean. As the flow non-uniformity increases towards the rear of the compressor, this difference can increase, depending on the sampling positions, resulting in an increased sampling error and consequently larger uncertainties in the compressor performance parameters. Equally, the same value of the sampling error at the rear of the compressor, implies a larger difference from the true circumferential mean than at the front of the compressor, since the mean levels of the stagnation pressure and the stagnation temperature have increased from the front to the rear of the compressor.

Since the efficiency is affected by sampling errors at two performance stations, while the flow capacity is only affected by the sampling errors at the local performance station, the increase in the error ranges for the efficiency is larger than for the flow capacity. The largest error ranges in the performance parameters are present in the rear performance block (S7-S8), in particular at the high flow capacity condition. While in the front and middle of the compressor, the circumferential flow non-uniformity is dictated by the upstream wake patterns, in the rear of the compressor, the driving mechanism is the potential field of the exit struts. As the circumferential flow non-uniformity upstream of the SND-struts increases at the high flow capacity condition, the sampling errors and consequently the efficiency uncertainty ranges increase. When the datum probe arrangement is used at the high-flow operating condition, the sampling errors at the leading edge of stator-7 are 0.46% (P_0) and 0.06% (T_0). At the leading edge of stator-8 the errors increase to 1.01% (P_0) and 0.10% (T_0). The resulting error range for the block pressure ratio is 2.95% and for the block temperature ratio 0.29%. The corresponding error range for the block efficiency amounts to nearly 40%. However, this values can be reduced to 15% when five probes at their optimum circumferential positions are used.

APPROXIMATION OF CIRCUMFERENTIAL SIGNALS USING SINGLE CIRCUMFERENTIAL HARMONICS

In the previous sections it has been shown that the sampling errors due to the circumferential variations in stagnation pressure and stagnation temperature have a significant influence on the error ranges of the performance parameters of the compressor. There is therefore a strong incentive to identify the circumferential probe positions which give as small as possible sampling errors before a new compressor is instrumented. Previously, the circumferential variations in stagnation pressure and stagnation temperature from the unsteady 180deg sector calculation were used to calculate the sampling errors. However, in practice, data from an unsteady large sector CFD calculation is generally not available during the instrumentation phase of a new test compressor. In this section, a method to reduce the sampling errors, which is based only on information available during the early stages of a test program is described.

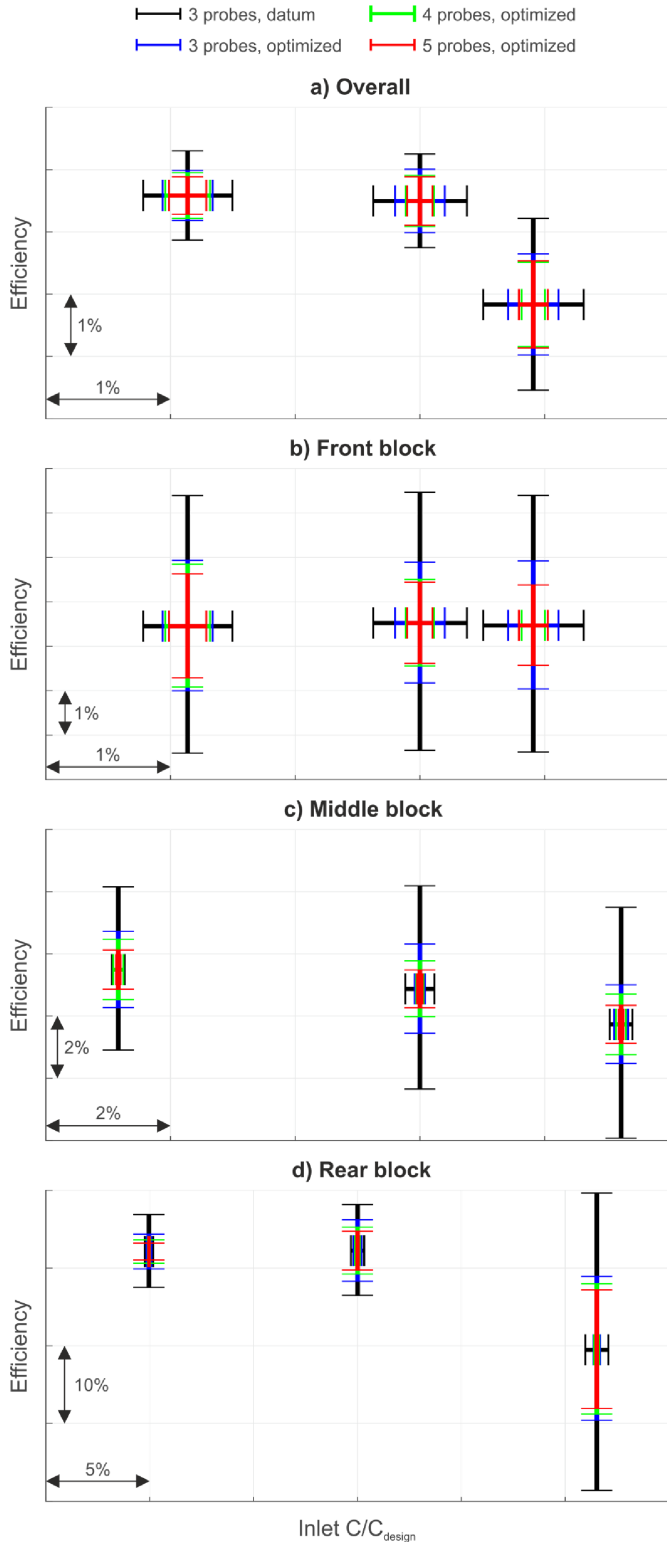


Figure 10: Error ranges of isentropic efficiency and inlet flow capacity due to sampling errors in P_0 and T_0 , overall (a) and individual performance blocks (b-d)

From the analysis of the circumferential signals it has been established that the dominant wave number is either associated with the wake pattern of the upstream stator row or the potential field of the large struts at the exit of the compressor. Actually resolving these wave numbers with circumferential probes would not be feasible. According to the Nyquist criterion, the number of circumferential samples would have to be at least twice the wave number which is to be resolved. For any engine-representative compressor, there are simply not enough stators to mount probes on to resolve the wake pattern from the upstream row. For the described test compressor, the potential field pattern of the exit struts could be resolved with a minimum of 16 instrumented stators. However, for the method described here, the wave numbers are prescribed, based on the knowledge gained in the previous sections, and therefore don't need to be resolved.

Assuming at least three circumferential data points to be known, a single harmonic can be constructed to approximate the circumferential variation. The locally dominant circumferential wave number is used for the harmonic approximation and the three data points are required to fix the mean, amplitude and phase of the harmonic. Instead of a single circumferential harmonic, an approximation based on two or more dominant wave numbers could theoretically be used. However, in this case, the relative amplitudes and phases of the individual harmonics would have to be specified and these signal characteristics are not known without a large-scale CFD solution. During the instrumentation phase of a new test compressor, an approximation based on a single wave number is therefore appropriate.

At first, it is useful to establish a reference level. For this, it is assumed that every vane within a stator row is instrumented. There are therefore more data points available than required for the construction of the single harmonic. To fit the single harmonic to the circumferential data points, a least-squares fit is used. The wave number of the single harmonic is taken to be the wave number of the wake pattern of the stator row directly upstream, except for the last stator row, for which the wave number of the exit strut potential field is used.

To illustrate this approach, data points are taken from the available CFD solution. The circumferential signals are sampled at every stator position. From the data points, the single harmonic is constructed and the mean value of the harmonic approximation and that of the circumferential CFD signal are compared. The differences for the stagnation pressure and the stagnation temperature are given in Table 3 in the form of error ranges. The limits of the ranges are given by the most and least favorable indexing positions at which the CFD signals are sampled, i.e. the relative positions of the sampling points relative to the circumferential non-uniformity. Since the actual positions of the probes relative to the flow non-uniformity are generally not known, error ranges as opposed to single values have to be given.

The errors in Table 3 can be compared with the errors from the previously described optimization process, which are shown in Figure 9. For the least favorable indexing position, the errors in stagnation pressure of the harmonic approximations and the

datum errors are of similar size. For the stagnation temperatures, the harmonic approximation errors are higher than those of the datum probe positions in the test rig. For the most favorable indexing position on the other hand, the errors from the harmonic approximations are over 65% smaller than those for the datum probe positions for both, stagnation pressure and stagnation temperature.

Table 3: Error ranges for the mean of the harmonic approximation from the mean of the original circumferential signal (CFD), all stator leading edges assumed to be instrumented, lowest and highest errors from indexing over one stator pitch

Stator	Flow pattern	P ₀ error [%]	T ₀ error [%]
S1	ESS IGV wake	0.07 - 0.31	0.01 - 0.11
S2	S1 wake	0.04 - 0.29	0.02 - 0.09
S3	S2 wake	0.05 - 0.26	0.01 - 0.09
S4	S3 wake	0.00 - 0.27	0.00 - 0.08
S5	S4 wake	0.03 - 0.21	0.01 - 0.08
S6	S5 wake	0.02 - 0.31	0.01 - 0.09
S7	S6 wake	0.00 - 0.10	0.00 - 0.04
S8	SND field	0.01 - 0.54	0.00 - 0.05

In a physical compressor test not every stator leading edge is instrumented. As described previously, it is common to use only a relatively small number of instrumented vanes per stator row. Based on the number of vanes in a given stator row and the wave number of the locally dominant circumferential flow non-uniformity, the circumferential size of the sector over which the probes are to be distributed can be defined. If the number of vanes and the dominant circumferential flow pattern have a common divisor, there is a repetition of the relative sampling position around the annulus. For the effective positioning of the probes, the sector size given by the greatest common divisor should be considered. For example, for a stator row with 42 vanes encountering a circumferential pattern of 26 wakes, the greatest common divisor is 2. For this configuration, the instrumented vanes should be all placed within one half of the annulus. All possible relative positions of the probes and the wake-pattern occur within one half of the annulus. In the other half of the annulus, the relative positions are repeated and no further information is gained. Within the calculated sector size, the probes are chosen to be equi-spaced.

To illustrate the approach, the flow entering stator-6 of the test compressor is considered. The wakes from stator-5 are taken as the locally dominant circumferential flow pattern. The number of vanes within stator-5 and stator-6 are known and their greatest common divisor can be calculated, which determines the fraction of the annulus over which the probes are to be distributed. In Figure 11, a choice of three, five and seven probes are shown to

be distributed over the calculated sector size. At the probe positions, the circumferential stagnation pressure and stagnation temperature signals from the CFD solution are sampled. From the sample points, the harmonic approximations are constructed again with a least-squares fit.

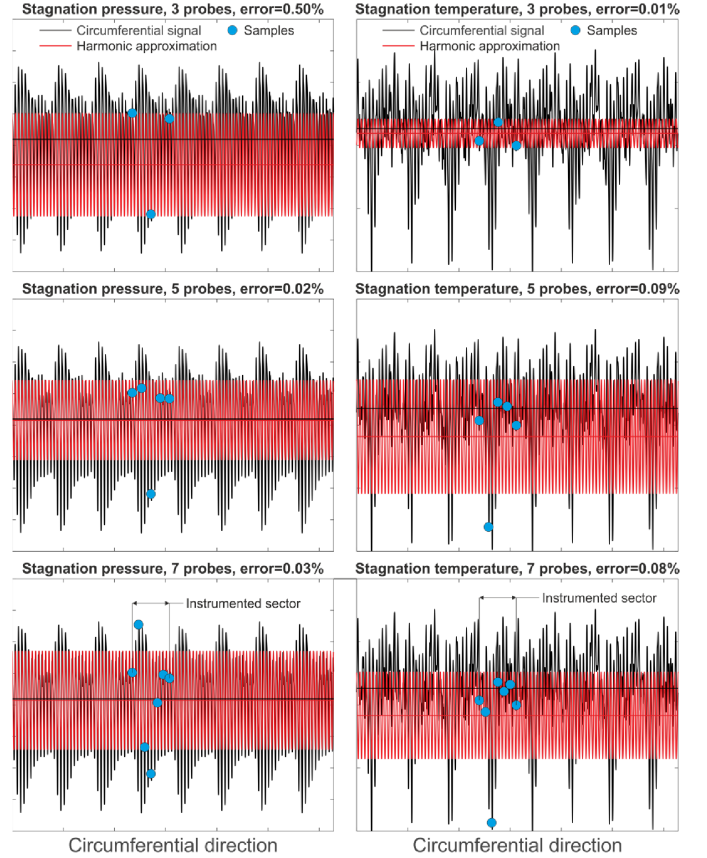


Figure 11: Approximation of circumferential signal with single harmonic, based on three, five and seven circumferential probes equi-spaced over instrumented sector, signals at stator-6 leading edge, wave number of stator-5 wake pattern used for approximation (design operating conditions, 50% height)

For the stagnation pressure, an error of 0.50% between the mean of the harmonic approximation and the mean of the CFD signal is achieved when the harmonic approximation is based on three data points. The error reduces to 0.02% and 0.03% for five and seven data points, respectively. These values are based on the most favorable indexing position of the data points. For the stagnation temperature, the error changes from 0.01% to 0.09% and 0.08% for three, five and seven data points. In this case, the least favorable indexing positions of the data points were chosen. This example shows that more equi-spaced probes do not automatically result in a smaller error. The reason for this is most obvious in the stagnation temperature plots. When five or seven

probes are used, one of the probes is sampling in an excursion of the signal, which is due to a lower harmonic. This outlying sampling point shifts the mean of the harmonic approximation away from the mean of the original signal, causing the error to increase.

This result of arriving at a higher error, when more circumferential probes are used, is counterintuitive. However, this result is derived from a single position of the instrumented sector within the circumference. To develop a more complete quantification of the error, it is necessary to increment the probe arrangement through the instrumented sector. The resulting circumferential variation of the error is shown for the stagnation pressure and the stagnation temperature in Figure 12. In addition to the errors for three, five and seven probes within the sector, the reference case, which assumes all stators to be instrumented, is shown. In contrast to the sparsely instrumented configurations, the reference case is circumferentially invariant. The error values quoted at the top of the plots in Figure 11 correspond to the values on the left border of the plots in Figure 12.

Figure 12 shows that the variations in the error reduce, as the number of probes in the sector is increased. For three probes, the standard deviation of the variations is 0.50% for the stagnation pressure and 0.07% for the stagnation temperature. As the number of probes is increased to five, the standard deviation reduces to 0.08% for the stagnation pressure and 0.03% for the stagnation temperature. With seven probes, a standard deviation of 0.04% is achieved for the stagnation pressure and of 0.01% for the stagnation temperature. The standard deviations are summarized in Table 4. As the limit of the maximum number of probes is approached, the standard deviation tends to zero and the error to the value of the reference case, for which every vane is instrumented.

Without the knowledge of the exact position of the probe configuration relative to the circumferential flow non-uniformity, a small number of probes can by chance result in a small error, which in fact can be smaller than the error for the limiting case with all vanes instrumented. But a small number of probes can also result in an unacceptably large error. In order to keep the uncertainty in the error as small as possible, a larger number of probes should be considered. In practice, the application of many probes needs to be balanced with their aerodynamic impact on the flow, the availability of supply paths as well as mechanical and financial constraints. The method of using a single harmonic to approximate the circumferential flow non-uniformity was described here using stator-6 together with the wake pattern of stator-5 as an example. However, the same approach is viable for the other stator rows of the present test compressor as well as for other multi-stage compressor configurations.

CONCLUSIONS

Time-averaged data (P_0 , T_0) from unsteady CFD calculations of a 180-degree sector of an 8-stage high-speed compressor was used to study the circumferential variations in the flow field and the stator-stator interactions. At design

operating conditions, circumferential variations in stagnation pressure of up 4.2% and up to 1.1% in stagnation temperature are predicted at mid-span. Fourier-decomposition of the circumferential signals showed that the locally most dominant influence stems from the wake-pattern of the stator row just upstream or from the potential field of the large SND-struts, if the local stator row is at the rear of the compressor.

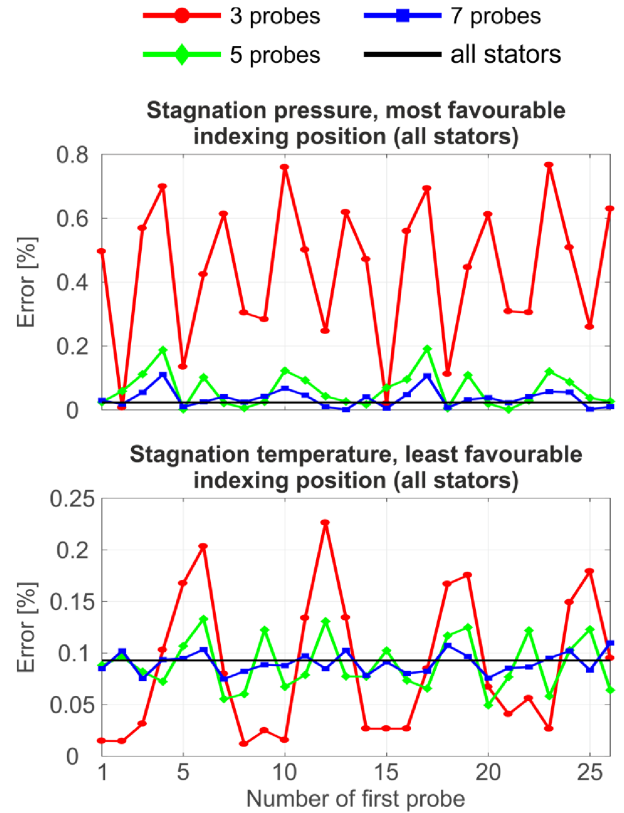


Figure 12: Circumferential variation of errors as equi-spaced probes are moved through instrumented sector, stator-5 wake pattern at stator-6 leading edge (design operating conditions, 50% height)

Table 4: Standard deviation for errors between harmonic approximation and original circumferential signal, stator-5 wake pattern at stator-6 leading edge

Stator row	Flow pattern	Flow variable	Circumferential probes		
			3	5	7
S6	S5 wake	P_0	0.50%	0.08%	0.04%
S6	S5 wake	T_0	0.07%	0.03%	0.01%

The values of the stagnation pressure and stagnation temperature acquired at a few stator leading edges of each row,

vary depending on the circumferential position within the non-uniform flow field. Using the CFD data and a metric for the error between the mean of a selected sample and the mean of the full circumferential signal, the circumferential sampling positions are optimised for each stator row. Compared to the probe positions used in a previous rig test, it is shown that the optimized probe positions reduce the local sampling error significantly – for some of the stator rows by more than half. Further reductions in the sampling error can be achieved when the number of circumferential probes is increased. The reductions in the sampling errors for P_0 and T_0 are converted into error margins for the isentropic efficiency and the flow capacity. These error margins are shown to reduce significantly, for most performance blocks by more than half, when the optimized probe positions are used instead of the datum probe positions.

A method for evaluating the sampling error based on single circumferential harmonics is presented. For this method, only the number of stators in each row has to be known. The method is therefore useful when large-scale unsteady CFD solutions are not available. For the approximation, the sector size of interest is determined based on the largest common divisor of the locally dominant wave number and the number of stators in the local row. It is demonstrated that the circumferential uncertainty of the resulting sampling error is reduced as the number of circumferential probes within the sector is increased.

ACKNOWLEDGMENTS

The authors would like to thank Rolls-Royce plc. for funding this study and for the permission to publish.

REFERENCES

- [1] Brandvik T. and Pullan G.: “An accelerated 3D Navier-Stokes solver for flows in turbomachines”, Proceedings of ASME Turbo Expo 2009, Turbomachinery Technical Conference and Exhibition, Orlando, Florida, USA, GT2009-60052.
- [2] Dodds J. and Vahdati M.: “Rotating stall observations in a high speed compressor, part 1: experimental study”, Proceedings of ASME Turbo Expo 2014, Turbomachinery Technical Conference and Exhibition, Düsseldorf, Germany, GT2014-25634.
- [3] Dodds J. and Vahdati M.: “Rotating stall observations in a high speed compressor, part 2: numerical study”, Proceedings of ASME Turbo Expo 2014, Turbomachinery Conference and Exhibition, Düsseldorf, Germany, GT2014-25635.
- [4] He L., Chen T., Wells R. G., Li Y. S. and Ning W.: “Analysis of rotor-rotor and stator-stator interferences in multi-stage turbomachines”, ASME Journal of Turbomachinery, Vol. 124, Oct. 2002, pp. 564-571.
- [5] Hewkin-Smith M. I., Pullan G., Grimshaw S. D., Greitzer E. M. and Spakovsky Z. S.: “The role of tip leakage flow in spike-type rotating stall inception”, Proceedings of ASME Turbo Expo 2017, Turbomachinery Technical Conference and Exhibition, June 26-30, Charlotte, North Carolina, USA, GT2017-63655.
- [6] Jameson A.: “Time dependent calculations using multigrid, with applications to unsteady flows past aerofoils and wings”, AIAA 91-1596, 1991.
- [7] Key N. L., Lawless P. B., Fleeter S.: “An experimental study of vane clocking effects on embedded stage performance”, ASME Journal of Turbomachinery, Vol. 132, Jan. 2010, 011018-1, GT2008-51087.
- [8] Kim S., Pullan G., Hall C. A., Grewe R. P., Wilson M. J. and Gunn E.: “Stall inception in low pressure ratio fans”, Proceedings of ASME Turbo Expo 2018, Turbomachinery Technical Conference and Exhibition, June 11-15, Oslo, Norway, GT2018-75153.
- [9] Liu Y., Lu L., Fang L. and Gao F.: “Modification of Spalart-Allmaras model with consideration of turbulence energy backscatter using velocity helicity”, Phys. Lett. A, 375 (24), 2011.
- [10] Shahpar S. and Lapworth L.: “PADRAM: Parametric design and rapid meshing system for turbomachinery optimization”, Proceedings of ASME Turbo Expo 2003, Turbomachinery Technical Conference and Exhibition, Atlanta, Georgia, USA, GT2003-38698.
- [11] Spalart P. R. and Allmaras S. R.: “A one-equation turbulence model for turbulent flows”, La Recherche Aérospatiale, 1:5-21, 1994.
- [12] Stummann S., Jeschke P., Metzler T.: “Circumferentially non-uniform flow in the rear stage of a multistage compressor”, Proceedings of ASME Turbo Expo 2015, Turbomachinery Technical Conference and Exhibition, Montréal, Canada, GT2015-42935.
- [13] Wang F., Carnevale M., di Mare L. and Gallimore S.: “Simulation of compressor at off-design conditions”, Proceedings of ASME Turbo Expo 2017, Turbomachinery Technical Conference and Exhibition, June 26-30, Charlotte, North Carolina, USA, GT2017-64964.
- [14] <https://www.hpc.cam.ac.uk/systems/wilkes-2>, Website of the Wilkes-2 GPU-cluster at the University of Cambridge, Jan. 2019.